Inductive sensor for lightning current measurement, fitted in aircraft windows - part I : analysis for a circular window

Inductive Sensor for Lightning Current Measurement, Fitted in Aircraft Windows—Part I: Analysis for a Circular Window

Alexander P. J. van Deursen, *Senior Member, IEEE*, and Vitality Stelmashuk

***Abstract*—A novel sensor is described for the detection of the lightning current through the fuselage of an aircraft. The sensor relies on the penetration of the magnetic field through fuselage openings and can be embedded in a window inside the aircraft. The sensor combines good sensitivity with sufficient bandwidth to record the lightning transient current. Guidelines for the position are derived from a mathematical analysis for a circular window.**

***Index Terms*—Aircraft, inductive sensor, lightning, viewport, window.**

I. Introduction

LIGHTNING is a real threat in flight [1], in particular during takeoff and landing. Statistically averaged, every aircraft has a chance of one lightning strike per year. The European project ILDAS [2] aims to develop and validate a prototype of a system capable to measure and reconstruct lightning current waveform in-flight, to localize the attachment points of the lightning and the current trajectory after strike, and to create a database of events. The acronym ILDAS is derived from "In-flight Lightning Strike Damage Assessment System." The goal is to assess the severity shortly after a lightning hit and to reduce maintenance time after landing. An extensive description is given in [3]. ILDAS is triggered by changes in the electric field at the aircraft. Sensors then determine the magnetic field induced by the current at twelve positions, retaining pre and post trigger data over the time span of 1 s. The selection of the number and positions of the sensors is described in [4]. After landing, the data are compared with possible field distributions derived for a number of current path scenarios [3], and the most likely is determined.

Three magnetic field sensors were developed [5]. The first is a small high-frequency (HF) coil with bandwidth up to 20 MHz to measure the strokes, similar to the one used in [6]. The second is a low-frequency (LF) coil to measure the small continuous current part of the lightning current. It is mounted inside a properly designed shield to discriminate the intense but fast magnetic field of the strokes. Both HF and LF coils with their integrators and data storage units are mounted at the outside of the aircraft, under covers or in fairings.

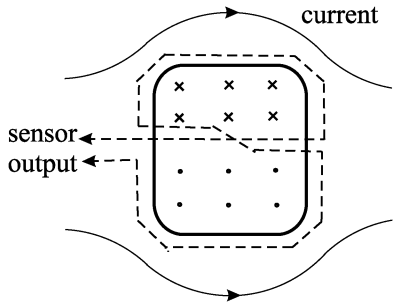

Fig. 1. Principle of sensor windings.

We proposed a third inductive sensor, which can be embedded in a window inside the aircraft. This sensor avoids protrusions that would obstruct the airflow around the fuselage. No signal feed-through passing the hull is needed either. The window sensor has good sensitivity and large bandwidth, but, as described here, a limited response at LF. The topic of this paper is the mathematical analysis of this sensor mounted on a circular window. The optimal sensor position is in the plane of the fuselage. The deviations of the sensitivity for less than optimal configurations has been analyzed mathematically to obtain information on critical points in sensor mounting procedures. A number of experimental studies have been carried out. First measurements have been performed on a small-scale mock-up, a tube with a hole in the wall. These are discussed in this paper. Second tests using the window sensor have been carried out on a Nimrod-size aircraft. The results have been presented earlier in [7]. The third series of tests were performed on an a fuselage mock-up in Cobham, as detailed in an internal ILDAS report. The final tests of the ILDAS system were performed in July 2009 on an A320 Airbus, and the positive outcome of good recognition of the strike points has been reported in [3]. The analysis of the data on the window sensor required accurate numerical modeling of the window. The details are presented in the accompanying paper [8].

II. Operating Principle

Fig. 1 shows a window as a rounded rectangle and a lightning current pattern in the fuselage around the window. The corresponding magnetic field enters the top half of the window

Manuscript received January 10, 2010; revised June 17, 2010; accepted June 17, 2010. Date of publication September 20, 2010; date of current version November 10, 2010. This work was supported in part by the European Union U FP6 Program under Contract 030806. The associate editor coordinating the review of this manuscript and approving it for publication was Dr. Patrick Ruther.

A. P. J. van Deursen is with the Department of Electrical Engineering, Eindhoven University of Technology, 5600 MB Eindhoven, The Netherlands (e-mail: a.p.j.v.deursen@tue.nl).

V. Stelmashuk was with the Department of Electrical Engineering, Eindhoven University of Technology, 5600MB Eindhoven, The Netherlands, on leave from the Institute of Plasma Physics, 18200 Prague 8, Czech Republic (e-mail: vitaliy@ipp.cas.cz).

Color versions of one or more of the figures in this paper are available online at http://ieeexplore.ieee.org.

Digital Object Identifier 10.1109/JSEN.2010.2055558

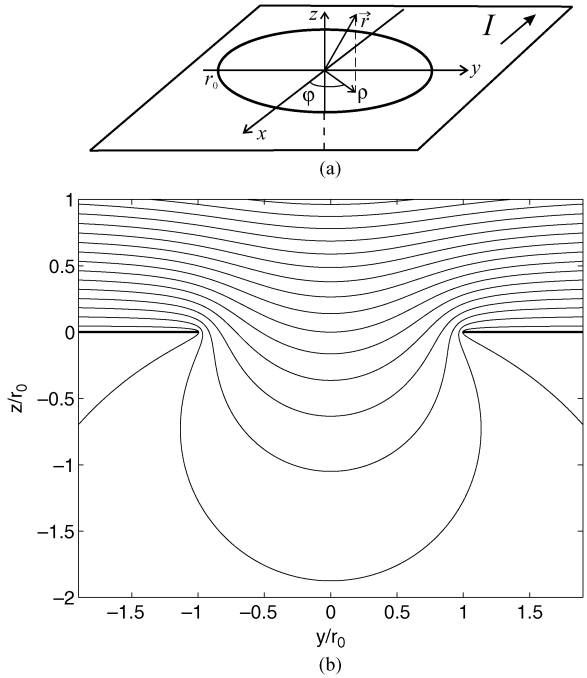

Fig. 2. (a) Coordinate system with respect to a circular hole of radius r_0 in a plane. (b) Diagram of field penetration through the circular hole. Above the plane, the magnetic field is homogeneous at large distance r.

and leaves through the lower half. A sensor coil is wound in the shape of a flattened figure-eight. The sensor wire follows the central bar twice. The outer perimeters is close to the fuselage at some distance from the window. Such a coil captures the magnetic flux entering and leaving the window and sums the induced voltages in each half. The sensor output is proportional to the magnetic field H_0 that would exist parallel to the fuselage without a window. For a (large) circular fuselage with radius R_f and a lightning current I one has the simple relation

$$H_0 = \frac{I}{2\pi R_f}. \tag{1}$$

Since R_f is much bigger than the window dimensions, the curvature of the fuselage can be neglected and an infinite conductive plane with circular hole can be assumed with a field H_0 at one side at large distance.

III. Mathematical Approach

Let us consider a circular hole with the radius r_0 instead of the rectangular window. The fuselage is regarded as a perfect conductor, i.e., no magnetic field penetrates the wall. The behavior of quasi-static fields near a circular hole in an infinitely large wall of infinite conductivity but zero thickness has been considered by Bethe [9] and reanalyzed by many authors; see, e.g., [10]. Applications range from hole coupling between waveguides to lenses for charged particle beams. We first used the approach and conventions by Kaden [11], who analyzed the magnetic field via an expansion in spherical harmonics. The coordinate system employed is shown in Fig. 2(a). Although pursued in [12], this approach appeared to be less well adapted for numerical evaluation because a large number of spherical harmonics are needed to describe the magnetic

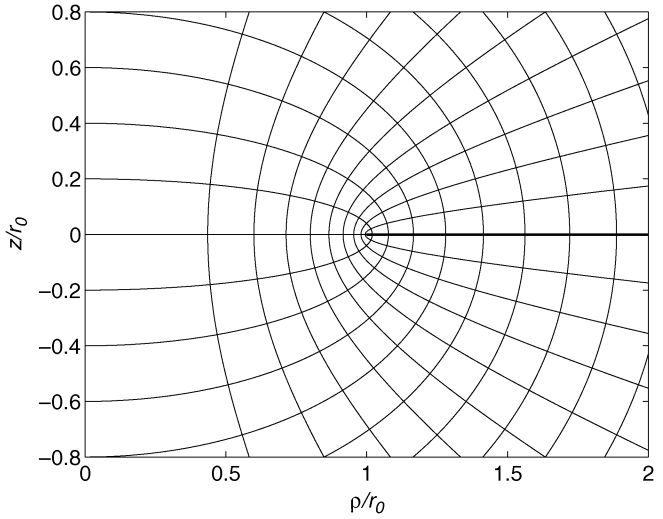

Fig. 3. Lines of constant elliptical coordinates (ξ, η), drawn in the plane of cylindrical coordinates (ρ, z).

potential. The higher harmonics cause fast oscillations, and as a result a slow convergence in integration if any at all. In two appendices, Kaden [11, Ch. H] proposes a second approach, referring to earlier work by Ollendorff [13, Sect. XIV]. Since both books are not available anymore and—to the authors' knowledge—these have not been translated into English, a compact description is given below, using the notation of [11]. The elliptical coordinates (ξ, η) are related to cylindrical ones (ρ, z)

$$\rho^2 = r_0^2\left[(1+\xi^2)(1-\eta^2)\right] \tag{2}$$

$$z = r_0\xi\eta, \tag{3}$$

with $-\infty < \xi < \infty$ and $0 \le \eta \le 1$, where $\xi > 0$ corresponds to $z > 0$ and $\xi < 0$ to $z < 0$; see also [14, Sect. 6.5]. Surfaces of constant η are hyperboloids through the hole; $\eta = 0$ corresponds to the plane $z = 0$, $\rho > r_0$ surrounding the hole. Constant ξ gives ellipsoids centered around $(\rho, z) = (0, 0)$; $\xi = 0$ corresponds to the plane $z = 0$ inside the hole. The focus of ellipsoids and hyperboloids is at $(\xi, \eta) = (0, 0)$, which is also $(\rho, z) = (r_0, 0)$. A set of shapes are drawn in Fig. 3, which shows that the coordinates themselves account for the diverging behavior of the fields near the focus. The inverse of the transformation for ξ reads

$$\xi^2 = \frac{-\left(r_0^2 - r^2\right) + \sqrt{\left(r_0^2 - r^2\right)^2 - 4r_0^2 z^2}}{2r_0^2}. \tag{4}$$

Here, we used $r = \sqrt{\rho^2 + z^2}$. The inverse transformation for η follows from (3). The closed-form expression of the scalar potential X is

$$X = \frac{1}{2}H_0\rho\left[1 + \frac{2}{\pi}\left(\arctan\xi + \frac{\xi}{1+\xi^2}\right)\right]\sin\varphi. \tag{5}$$

This potential satisfies the boundary conditions for the magnetic field $H = \nabla X$: 1) at the fuselage ($z = 0$, $\rho > r_0$), the perpendicular component is zero; 2) for large distances outside the

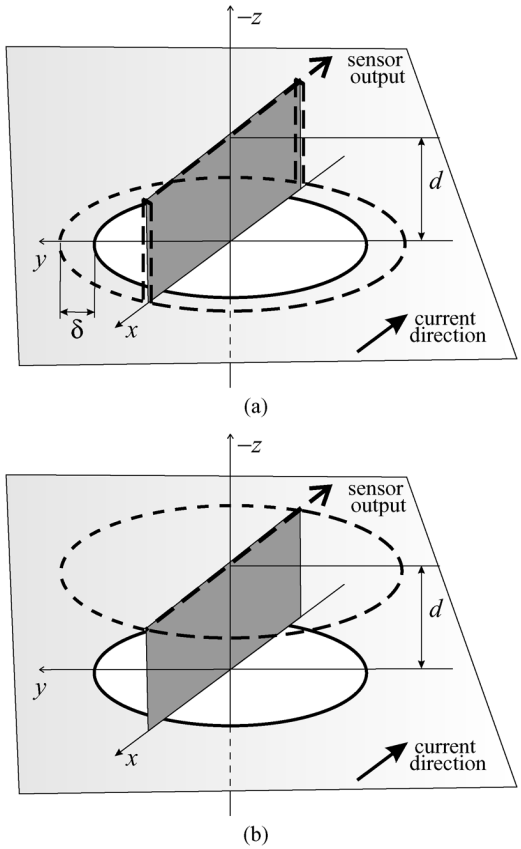

Fig. 4. (a) Sensor (dashed line) against the fuselage, with the central bar shifted over the distance d and extended over the length δ. (b) Sensor fully lifted. The drawings shows the inside of the fuselage, and the coordinate system is placed upside down.

fuselage ($z \gg 0$, H approaches H_0); and 3) inside ($z \ll 0$), H tends to zero as a dipole field. The flux Φ through a surface S is calculated as the integral

$$\Phi = \mu_0 \iint_S \nabla X \cdot \hat{n} dS \tag{6}$$

where $\hat{n}$ is the unit vector on the surface S.

IV. Selected Sensor Shapes

Three shapes of the figure-eight coil will be analyzed, which are given here:

1) flat sensor in the plane of the fuselage;
2) sensor with the central bar shifted inside the aircraft over the distance d [see Fig. 4(a)];
3) flat sensor completely shifted over the distance d [see Fig. 4(b)].

The different shapes allow to study the changes of the sensor sensitivity when obstructions prohibit the optimal shape 1). It is instructive to look at the magnetic field inside the hole that can be calculated analytically. The perpendicular component is

$$H_z = \frac{\partial X}{\partial z} = \left.\frac{\partial X}{\partial \xi}\right|_{\rho=c.} \times \left.\frac{\partial \xi}{\partial z}\right|_{\rho=c.} \tag{7}$$

with the derivatives taken at constant ρ and at $z = 0$, and $\xi = 0$. The first term in the right-hand side product of (7) is $2H_0\rho/\pi$. The second term is obtained by differentiating (3) to yield

$$\left.\frac{\partial z}{\partial \xi}\right|_{\rho=c.} = r_0\eta + r_0\xi \left.\frac{\partial \eta}{\partial \xi}\right|_{\rho=c.}. \tag{8}$$

For $\xi = 0$, the second term on the right-hand side of (8) vanishes. The final result is

$$H_z(\rho < r_0, z = 0) = \frac{2H_0}{\pi} \frac{\rho}{\sqrt{r_0^2 - \rho^2}} \sin\varphi. \tag{9}$$

The in-plane component H_t is homogenous, oriented parallel to the y-axis, and of magnitude

$$H_t = H_0/2. \tag{10}$$

A. Flat Sensor in the Plane

With the sensor against the fuselage plane, there is no flux between the outer perimeter of the figure-eight and the fuselage. The magnetic flux through a sensor of radius $\rho_s < r_0$ is obtained by integration of H_z over the quarter circle and multiplying by 4 to yield

$$\Phi_{\rho_s} = \frac{4\mu_0 H_0 r_0^2}{\pi} \left[\arcsin\frac{\rho_s}{r_0} - \frac{\rho_s}{r_0}\sqrt{1 - \frac{\rho_s^2}{r_0^2}}\right]. \tag{11}$$

For a sensor with $\rho_s \geq r_0$, one arrives at

$$\Phi_0 = 2\mu_0 H_0 r_0^2. \tag{12}$$

The square-root term in (11) causes a fast decay in sensitivity for ρ_s slightly smaller than r_0. This result holds for an infinitely thin plane. Changes at the edge, for instance, a small rim, have large influence on Φ_0. On the other hand, Φ_0 does not depend on ρ_s as long as it is larger than r_0 and the coil wire is against the fuselage. The sensitivity does not strongly vary with the position of the central bar near the line $y = 0$ in $z = 0$ plane because the H_z is zero there. For a displacement of the central bar by the amount e in the y-direction, the sensitivity varies as

$$\frac{\Phi(e)}{\Phi_0} = 1 - \left(\frac{e}{r_0}\right)^2 \tag{13}$$

which is easily verified by rewriting (9) in Cartesian coordinates.

B. Central Bar Shifted

As shown in Fig. 4(a), the central bar can be shifted to the position $z = -d$. Assume that vertical leads at $\rho = r_0$ connect the wires in the bar with the perimeter of the sensor. A quick estimate of the reduction in sensitivity is possible. The horizontal field $H_y = H_t$ near the central bar is equal to $H_0/2$. For small d, the flux through the rectangle formed by the central bar at

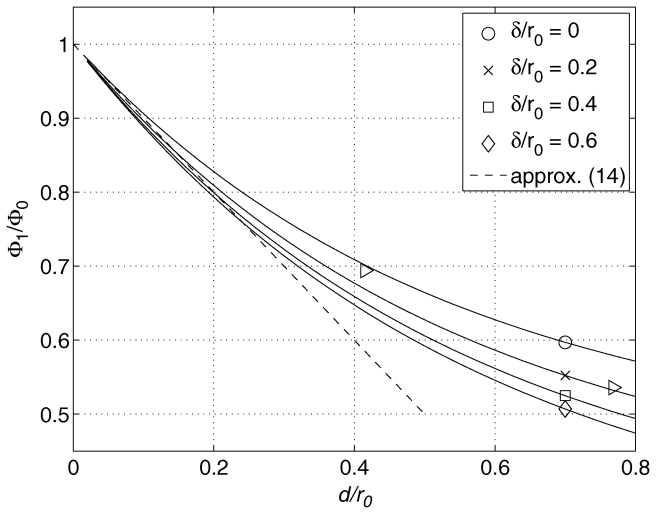

Fig. 5. Sensitivity of the sensor as function of shift d of the middle bar, for four different extensions δ of the bar. When $d \to 0$, all curves merge with the approximation (14). The markers at $d/r_0 = 0.7$ are indicators for the legend. The markers ▷ are discussed in Section V.

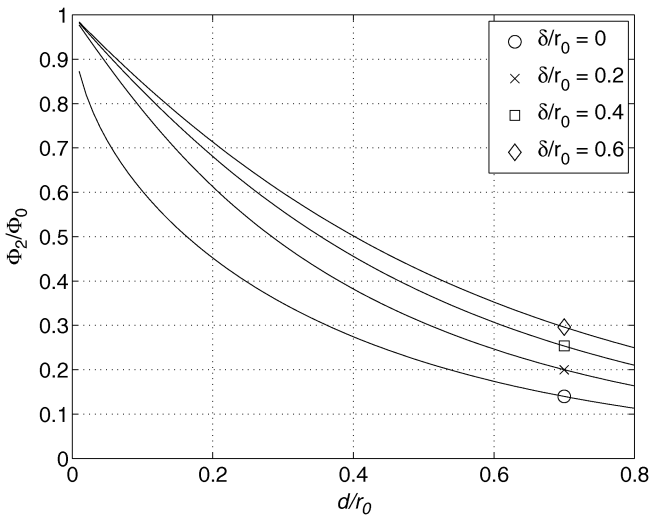

Fig. 6. Sensitivity of the sensor as function of shift d of the whole sensor, for four different extensions δ of the sensor radius. Please note that the sensitivity drops faster than in Fig. 5, in particular for $\delta = 0$.

$z = -d$ and at $z = 0$ is $\mu_0 H_0 r_0 d$, which is missed twice by the sensor. A first approximation of the sensitivity reduction is

$$\frac{\Phi_{1a}(d)}{\Phi_0} \approx 1 - \frac{d}{r_0} \tag{14}$$

which overestimates the actual reduction at larger d. When the central bar is shifted over the distance d, the flux Φ_m not seen by the figure-eight sensor is

$$\frac{\Phi_m(d,\delta)}{\mu_0} = 4 \int_0^d \mathrm{d}z \int_0^{r_0+\delta} H_\varphi \mathrm{d}\rho \tag{15}$$

where $H_\varphi = \partial X/\rho\partial\varphi$ evaluated at $\varphi = 0$. We used an upper limit $r_0 + \delta$ in the integration over r, since the sensor central bar may be extended over the window radius r_0 by a distance δ; see Fig. 4(a). The radius of the figure-eight, which is laying against the fuselage, is increased similarly. Fig. 5 shows the resulting sensitivity $\Phi_1 = \Phi_0 - \Phi_m$ as a function of distance d for four values of the extension δ. The numerical results have been obtained with Mathematica.[1] The divergence of the field at $(\rho, z) = (r_0, 0)$ did not pose particular problems in the integration.

C. Shifted Sensor

If the full sensor is shifted over the distance d, then the flux through the cylinder between the sensor outer perimeter and fuselage is missed. The sensitivity can now be partially restored by increasing the outer perimeter to the radius $r_0 + \delta$. It is convenient to calculate the flux through the sensor directly via the quarter circle

$$\frac{\Phi_2(d,\delta)}{\mu_0} = 4 \int_0^{\pi/2} \mathrm{d}\varphi \int_0^{r_0+\delta} H_z \rho \mathrm{d}\rho. \tag{16}$$

[1]Online. Available: http://www.wolfam.com.

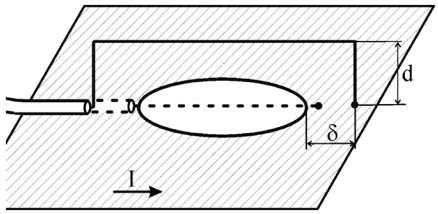

Fig. 7. Single-turn version of the window sensor, made by a coaxial signal cable extending the inner lead over the hole.

The resulting Φ_2 is shown in Fig. 6. The sensitivity of the sensor decreases approximately twice as fast with increasing d as the previous sensor with only the central bar shifted (Fig. 5) because of the strong field near the circle edge, midway between the central bar ends; see Fig. 2(b). The strong field causes a substantial loss for a sensor that remains even close to the edge. The flux missed by the sensor is approximately proportional to $\sqrt{d}$, as shown by the steep increase of the curve for small d and $\delta = 0$, which is similar to (11).

V. Sensor Validation

A brass tube of $r_t = 0.45$ m in diameter and 1.5 m in length acted as fuselage mock-up. The tube is used inside-out, as it is excited internally by a thin wire near the axis with the tube as return. An 82-mm-diameter hole was made at midlength in the tube. A single-turn version of the window sensor was mounted; see Fig. 7. The sensor wire was on the outside and was mounted midway over the window at three distances d: 0, 17, and 32 mm or $d/r_0 = 0$, 0.42, and 0.76, respectively. The distance δ was 8.5 mm or $\delta/r_0 = 0.2$. The tube also acted as a return for the measuring circuit. We measured the induced sensor voltages caused by an excitation current of $I = 2.1$ A at 500 kHz through the inner lead: U_0, U_{17}, and U_{32}. The ratios of the voltages U_{17}/U_0 and U_{32}/U_0 are plotted in Fig. 5 by the markers ▷.

In a second set of measurements, we determined the coupling between the inner circuit and the sensor by a network analyzer HP 4396A with the S-parameters set HP 85046A over the frequency range up to 10 MHz. The sensor wire was at the distance $d = 1.5$ mm from the tubes cylindrical surface. Fig. 8 shows the

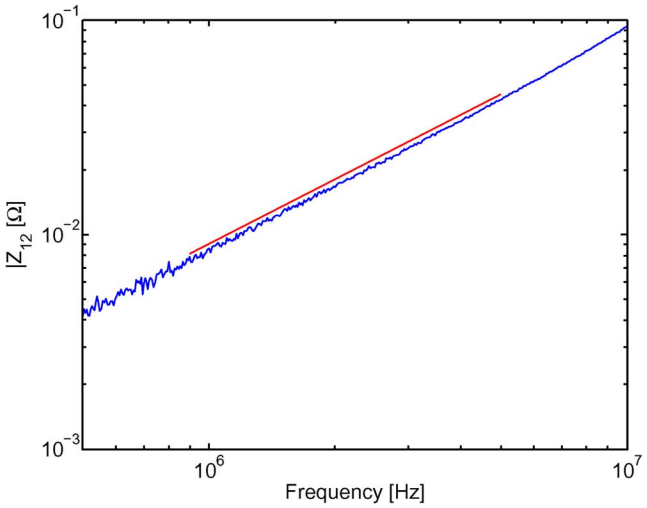

Fig. 8. Coupling impedance $|Z_{12}|$ between the excitation circuit inside the tube and the sensor, measured by a network analyzer. The straight line represents the analytical approximation ωM_a.

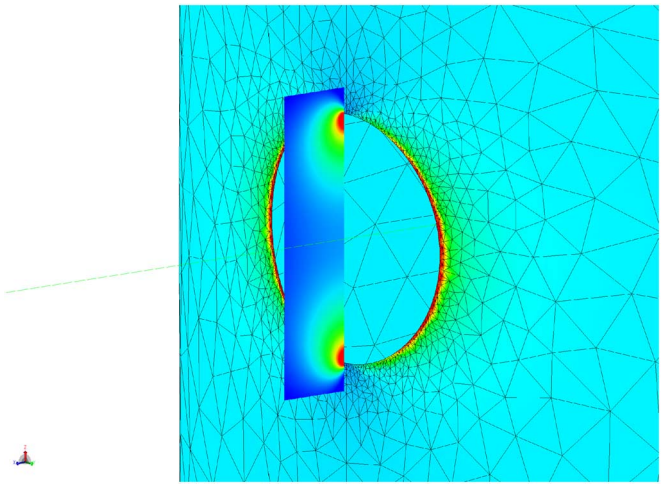

Fig. 9. Meshing, current density in the tube and z-component of the electric field in the rectangular portion of the $y = 0$ plane near the hole. The tube axis extends along the z-direction; the x-axis is normal to the plane of the hole. Color is available online only.

coupling as transfer impedance Z_{12}. The experimental coupling inductance M_e has been determined by a fit to $|Z_{12}| = \omega M_e$ between $f_1 = 0.9$ MHz and $f_2 = 5$ MHz. This range was chosen because of the noise below f_1, and the steeper increase above $2f_2$ caused by the onset of traveling wave effects in the tube. Approximate analytical expression of M_a follows from the inside field $H_0 = I/2\pi r_t$ without the hole

$$M_a = \frac{\mu_0}{2\pi r_t}\left(r_0^2 - d \times r_0\right) \tag{17}$$

which assumes that the tube wall can be considered flat near the window. The resulting Z_{12} is displayed by the solid straight line in Fig. 8. Alternatively, one can express the sensitivity in effective flux capturing area A: $V = \mu_0 A \partial H_0/\partial t$. The agreement between M_e and M_a is within 7%; see Table I. This is acceptable if one considers the limitations of the simple model, the mechanical tolerances on the actual tube, and the accuracy of the analyzer and S-parameters set (0.4 dB, equivalent to 5%).

The tube wall thickness was 1.5 mm; the finite thickness rounds the edge divergence and reduces the flux. We approximated the actual wall surface near the edge by an equi-flux surface with a smallest radius of curvature equal to half the wall thickness. The sensor sensitivity was reduced by about 15% for $d = 0$. This approach clearly overestimates the edge effect.

Also, the position of the lead inside the tube turned out to be influential. An offset o from the axis in the direction of the sensor causes the field variation $\Delta H_0/H_0 = 2o/r_t$) at the inside wall of the tube. A distance of 1 mm larger from the hole would cause approximately a 1% smaller M.

In order to determine the influence of the limited diameter of the tube, we modeled the tube with hole in a FEKO Method of Moment (MoM) approach.[2] On the tube, the triangular element sides were 3 cm, which made the set of triangles deviate from the cylindrical surface by 0.5 mm at most. The triangle sides decreased to 1 mm near the edge of the hole to deal with the diverging current and charge density there. As excitation, we used two voltage sources of opposite phase at the ends of the inner wire. This arrangement ensured a predominant inductive E-field near the sensor. A fixed frequency of 2 MHz was selected. Fig. 9 shows the amplitude of E_z and of current density over the relevant surfaces. Of course, the momentaneous values are 90° out of phase. The sensor voltage was then determined by trapezoidal integration of the electric field over the line at 1.5 mm from the hole center, extending over 8.5 mm as in the measurements. Table I also shows the resulting coupling inductance $M_m = |V/I\omega|$. The 1% agreement with M_a shows that the curvature of the tube had little influence on the window sensor. As an additional check, we observed that the parallel component of the magnetic field H_y is near to constant and equal to $H_0/2$ to within 1% over the central line of the hole, in agreement with (10).

[2]Online. Available: http://www.feko.info/.

TABLE I
VALUES FOR M IN nH AND A IN UNITS r_0^2. SUBSCRIPT e STANDS FOR EXPERIMENTAL, a FOR ANALYTICAL, AND m FOR MOM MODEL

M_e	A_e	M_a	A_a	M_m	A_m
1.34	0.90	1.440	0.963	1.455	0.974

As mentioned in the Introduction, the window sensor has been tested on a Nimrod airplane [7]. The wave shape of the current injected on the aircraft was correctly reproduced. Small deviations were caused by the nonideal transfer function of passive integrator in the signal conditioning path. The amplitude was less than the assumed sensitivity, mostly because of the placement of the outer perimeter of the figure-eight inside the window opening, rather than against the fuselage. Here, we refer to [7, Fig. 7].

VI. CONCLUSION

We proposed the figure-eight sensor that can be mounted in a window inside the aircraft. The advantages are: a good sensitivity proportional to the area, ease of installation, and absence of feedthroughs in the fuselage. Also the sensor bandwidth compares well with the one for a small multiturn coil [5]. The outer perimeter of the figure-eight coil should preferentially be laid

against the fuselage, at some distance of the window. The analysis presented shows how sensitivity depends on the coil position and shape assuming a homogeneous field outside the aircraft. The central bar may obstruct the view through the window. Thin wires or translucent material such as indium–tin oxide on the widow pane may reduce this inconvenience. A coil with only central bar shifted to some distance of the window seems acceptable. If the whole coil is shifted, the sensitivity depends strongly on the distance. Since the sharp window edge and the associated diverging field do not occur in practice, the sensitivity should be carefully considered for actual sensors. A nonhomogeneous outside field may occur when other nearby conductors are present. The analysis of the window sensor for such fields was outside the scope of this work. The window sensor has similarities with Janus' head: it looks to and is equally sensitive to magnetic fields generated inside the aircraft. However, the lightning-induced fields are often more intense and can be recognized easily.

Applications are not limited to aircraft. Lightning current measurements on towers for television or for windmills often rely on Rogowski (R.) coils. Ideally, an R. coil fully encircles the tower at the outside, and its output is then strictly proportional to $\partial I/\partial t$. Being outside the tower, the R. coil itself is exposed to lightning. A large single coil is often inconvenient, and it is replaced by a number of smaller segments, each sensitive to the local magnetic field. The signals from the segments are then added. In such a case, the window sensor may also be used on any available opening in the tower. Other applications can be imagined as well: coaxial structures, such as occur in pulsed power setup. If even minute openings in the wall were available, the sensor could be placed there.

ACKNOWLEDGMENT

The authors would like to thank all ILDAS partners for their cooperation during the project.

REFERENCES

[1] M. Uman and V. Rakov, "The interaction of lightning with airborne vehicles," *Progr. Aerosp. Sci.*, vol. 39, pp. 61–81, Oct. 2003.
[2] [Online]. Available: http://ildas.nlr.nl/. Amsterdam, The Netherlands
[3] R. Zwemmer, M. Bardet, A. de Boer, J. Hardwick, K. Hawkins, D. Morgan, M. Latorre, N. Marchand, J. Ramos, I. Revel, and W. Tauber, "In-flight lightning damage assessment system (ILDAS); results of the concept prototype tests," in *Proc. Int. Conf. ICOLSE*, Pittsfield, 2009, Paper AAA-1.
[4] S. Alestra, I. Revel, V. Srithammavanh, M. Bardet, R. Zwemmer, D. Brown, N. Marchand, J. Ramos, and V. Stelmashuk, "Developing an in-flight lightning strike damage assessment system," in *Proc. ICOLSE*, Paris, France, 2007, Paper Ico7/PPR33.
[5] V. Stelmashuk, A. van Deursen, and R. Zwemmer, "Sensor development for the ILDAS project," in *Proc. EMC Europe Workshop*, Paris, France, Jun. 2007.
[6] P. Lalande, A. Broc, P. Blanchet, S. Laik, S. Luque, J.-A. Rouquette, H. Poirot, and P. Dimnet, Onera, in *Proc. In-Flight Lightning Measurement System: Design and Validation*, Toulouse, France, 2003, EM-Haz-Onera Rep05.
[7] V. Stelmashuk, A. van Deursen, and M. Webster, "Sensors for in-flight lightning detection on aircraft," in *Proc. EMC Europe Symp.*, Hamburg, Germany, Sep. 2008, pp. 269–274.
[8] A. van Deursen, "Inductive sensor for lightning current measurement, fitted in aircraft windows—Part II: Measurements on an A320 aircraft," *IEEE J. Sensors*, this issue.
[9] H. Bethe, "Theory of diffraction by small holes," *Phys. Rev.*, vol. 66, pp. 163–182, Oct. 1944.
[10] J. Jackson, *Classical Electrodynamics*. Chichester, U.K.: Wiley, 1999.
[11] H. Kaden, *Wirbelströme und Schirmung in der Nachrichtentechnik*. Berlin, Germany: Springer, 1959.
[12] V. Stelmashuk and A. van Deursen, "Sensors for lightning measurements on aircraft," in *Proc. IEEE Sensors*, Lecce, Italy, 2008, pp. 1036–1039.
[13] F. Ollendorff, *Potentialfelder der Elektrotechnik*. Berlin, Germany: Springer, 1932.
[14] G. Korn and T. Korn, *Mathematical Handbook for Scientists and Engineers*. New York: MacGraw-Hill, 1964.

Alexander P. J. van Deursen (A'97–SM'97) received the Ph.D. degree in physics from Radboud University, Nijmegen, The Netherlands, in 1976.

He was a Postdoctoral Researcher with the Max Planck Institut fur Festkörperforschung, Hochfeld Magnetlabor, Grenoble, France. He returned to Nijmegen, where he worked on solid-state physics on electronic structures of metals, alloys, and semiconductors by high magnetic field techniques. In 1986, he joined the Eindhoven University of Technology, Eindhoven, The Netherlands, and shifted his attention to electromagnetic compatibility (EMC). He has also been engaged in several International Electrotechnical Commissions (IEC) working groups. He has been the Chairman and member of different committees in international conferences. He is a member of the International Steering Committee of EMC Europe and is Vice-Chairman of URSI Commission E.

Vitality Stelmashuk received the Ph.D. degree in plasma polymerization from Charles University, Prague, Czech Republic, in 2004.

Since 2003, he has been with the Institute of Plasma Physics, Academy of Sciences of the Czech Republic, Prague. His research work included water discharge and generation of focused shock waves in water for medical applications. He was a Postdoctoral Researcher with the Eindhoven University of Technology, Eindhoven, The Netherlands, in the group EPS from 2006 to 2009, working on the ILDAS project. He returned to Prague, where he continues to work on water discharge and its medical applications.